ACS APPLIED MATERIALS & INTERFACES

Research Article

www.acsami.org

Combined Strategy to Realize Efficient Photoelectrodes for Low Temperature Fabrication of Dye Solar Cells

A. Alberti,*[,†] L. De Marco,[§] G. Pellegrino,[†] G. G. Condorelli,[‡] R. Giannuzzi,[§] R. Scarfiello,[§] M. Manca,[§] C. Spinella,[†] G. Gigli,[§,∥,⊥] and A. La Magna[†]

[†]CNR-IMM Zona industriale, Strada VIII 5, 95121, Catania, Italy

[‡]Università degli Studi di Catania and INSTM UdR Catania; Viale Andrea Doria 6, 95124 Catania, Italy

[§]CBN, Center for Biomolecular Nanotechnologies, Fondazione Istituto Italiano di Tecnologia—Energy Platform Via Barsanti, 73010 Arnesano, Lecce, Italy

[∥]National Nanotechnology Laboratory (NNL), CNR Istituto Nanoscienze, c/o Distretto Tecnologico, Via Arnesano km 5, 73100 Lecce, Italy

[⊥]Dipartimento di Matematica e Fisica "E. De Giorgi", Università del Salento, via per Arnesano, 73100 Lecce, Italy

ABSTRACT: We implemented a low-temperature approach to fabricate efficient photoanodes for dye-sensitized solar cells, which combines three different nanoarchitectures, namely, a highly conductive and highly transparent AZO film, a thin TiO_2-blocking layer, and a mesoporous TiO_2 nanorod-based working electrode. All the components were processed at $T \leq 200°C$. Both the AZO and the TiO_2 blocking layers were deposited by reactive sputtering, whereas the TiO_2 nanorods were synthesized by surfactant-assisted wet-chemical routes and processed into photoelectrodes in which the native geometric features assured uniform mesoporous structure with effective nanocrystal interconnectivity suitable to maximize light harvesting and electron diffusion. Because of the optimized structure of the TiO_2-blocking/AZO bilayer, and thanks to the good adhesion of the TiO_2 nanorods over it, a significant enhancement of the charge recombination resistance was demonstrated, this laying on the basis of the outstanding power conversion efficiency achievable through the use of this photoanode's architecture: a value of 4.6% (N719) was achieved with a 4-μm-thick electrode processed at $T = 200°C$. This value noticeably overcomes the current literature limit got on AZO-based cells (N719), which instead use Nb-doped and thicker blocking layers, and thicker nanostructured photoanodes, which have been even sintered at higher temperatures (450−500°C).

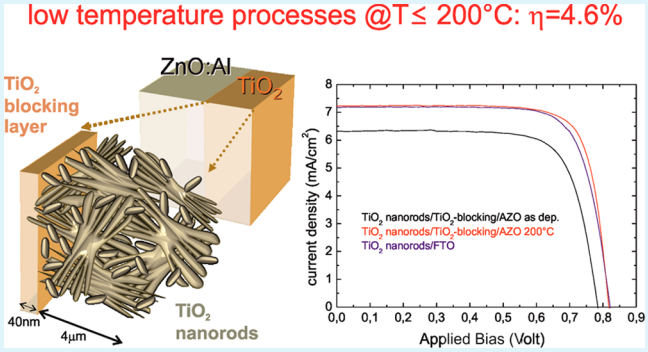

KEYWORDS: *DSSC, blocking layer, TiO_2 anatase-nanorods, AZO, sputtering*

1. INTRODUCTION

Dye-sensitized solar cells (DSSCs) have been receiving increasing interest in the research, as well as in the industrial frameworks. A number of manufacturers have begun investing in this sector, driven by the prospected short payback period, by the simple manufacturing processes, and by the possibility of also using the technology in building-integrated photovoltaics (BIPV), that Si-based solar cells do not offer. Nowadays, the BIPV is one of the fastest growing segments of the photovoltaic industry. In the standard scheme of the photo-anode of a DSSC, proposed by Gratzel,[1] a mesoporous thin film of nano-sized TiO_2 crystals (nano-paste) is deposited on a transparent conductive oxide (TCO), and sensitized by a photoactive dye.[2]

TiO_2 in the anatase polymorphism is the most appropriate material for such applications mainly since it offers a high chemical stability, a proper surface reactivity towards a large choice of light harvesting dyes, and good carrier transport properties. Among the TCOs, Al-doped Zn oxides (AZO) are recently becoming attractive candidates thanks to the abundance and nontoxicity of the elements and to the versatility of the doping procedure.[3] The AZO substrate serves as collector of the carriers injected through the dye/TiO_2 interface. In this respect, it is well known that the AZO structural properties (e.g., texturing, Al content) and the surface exposed to the TiO_2 deposition[4,5] are crucial to tailor the behaviour of the cell. AZO layers can offer low resistivity (<mΩ × cm), high mobility values, and high transparency in the visible range (up to 90% transmittance, or even higher); moreover AZO is more resistant to hydrogen plasmas, has a better thermal stability and lower cost with respect to the commonly used transparent conductive materials (TCM; e.g., FTO, ITO[3]).

Received: December 19, 2013
Accepted: April 2, 2014
Published: April 2, 2014

   dx.doi.org/10.1021/am4058524 | *ACS Appl. Mater. Interfaces* 2014, 6, 6425−6433

Recently, it has been argued that the use of a uniform layer between the AZO substrate and the mesoporous TiO_2 can improve the cell performances. TiO_2 intralayers would serve to several purposes:[6−10] to protect the AZO surface against corrosion by the electrolytic solution (protective layer); to improve the electrical coupling between the nanopastes and the AZO surface (coupling layer); and to reduce the back-recombination process of the injected carriers (blocking layer). AZO-based DSSCs which employ blocking/protective TiO_2 layers, have, up to now, reached efficiencies in the range between 1.9% and 3.8% with N719 as dye. The maximum value was got by using a Niobium-doped TiO_2 blocking layer (e.g., 100 nm) over AZO[11] or over AZO/Ag/AZO multilayer structures.[12] The TiO_2:Nb layer was found to block oxygen diffusion into AZO during air-annealing and to suppress the formation of Zn^{2+}-dye aggregates at the AZO surface. In all those cases, a thermal budget in the range of 450−500 °C is needed for the TiO_2 nanopaste sintering process.

To improve the blocking layer performances and to extend them to the low temperature regimes, as required for production of cells on flexible substrates, a further reduction of the blocking layer thickness and the TiO_2 crystallization under ∼200°C are mandatory issues. TiO_2 crystallization in the anatase polymorphism is not easy to be got at such low temperatures for standard deposition processes.[13] It has been reported[14] that by using reactive pulsed magnetron sputtering on unheated substrates the structure of the deposited layer can be tuned from amorphous to partially crystallized by increasing the oxygen percentage (e.g., 17%) in the deposition chamber. Since an induced heating at the sample surface is expected because of the plasma and deposition process itself,[15] the surface temperature can reach 160 °C (or even more than that), and anatase can be consequently formed under other specific conditions, such as short anode−cathode distances (e.g., 6 mm), high layer thickness (e.g., ≥500 nm), high magnetron currents (e.g., ≥2 A), power loading ≥7 W/cm^2 on ceramic targets and ≥20 W/cm^2 on conductive (heating dissipating) targets.

A key goal is, therefore, the development of a controlled and reproducible process to induce low temperature TiO_2 crystallization in thin layers (<100 nm). With respect to conventional chemical approaches, the use of sputtering equipment would actually offer huge advantages in terms of reproducibility of the process and realization of multiple blocking-TiO_2 /AZO bilayers (anodes) on large areas in a single-run process. This would guarantee a very high production throughput which is mandatory to reduce the cost of the cells. Add to this also the fact that nowadays the purchasing of the conductive glass (e.g., covered by ITO) represents about the 50% of the cost of the actual devices, and therefore, using home-made AZO layers as substrate for the blocking-TiO_2 would represent a huge advantage for production purposes.

Another key issue is the quality (in terms of surface to volume ratio and interconnectivity) of the mesoporous TiO_2 layer deposited on the blocking TiO_2, which plays an important role in the light harvesting, to reduce recombination dynamics and, therefore, it is crucial to determine the photoelectrochemical properties of the system. Although a porous electrode made of spherical nanocrystallites with high surface area guarantees the loading of large amounts of dye molecules, the diffusion of electrons can be restricted by trapping and detrapping events along defects, surface states, and grain boundaries. An attractive way to improve the charge collection efficiency is the use of anisotropically shaped TiO_2 nanostructures, such as all-linear or branched nanorods,[16−18] which are able to provide extended directional pathways for rapid collection of photogenerated electrons.

In this paper, we explore an approach based on the use of TiO_2-nanorods/TiO_2-blocking/AZO multilayers to realise DSSC's photoanodes at low thermal budget. A particular care was spent to optimise the structural properties of the single photoanode components and of the involved interfaces. To that purpose, the TiO_2-blocking/AZO bilayer was deposited by sputtering, while the mesoporous film of one-dimensional TiO_2 building blocks was realised by the deposition of printable colloidal pastes composed of nanorods synthesized by surfactant-assisted routes. In particular, the mesoporous photoanodes consist of two different breeds of nanorods: high aspect-ratio, hyperbranched 150 nm-sized nanorods guaranteed superior electron transport properties while small nanorods (5 × 40 nm sized) provided tremendous dye loading capability.

In the paper, it is discussed how the TiO_2-blocking layer, which is ∼40 nm-thick and dopant-free, has a crucial role in the cell performances, particularly evidenced by using soft post-deposition thermal treatment at 200 °C. The process is compatible with newly designed heat-stabilized PEN substrates.[19,20] With our approach, a high conversion efficiency was got, despite the low thermal budget used with respect to those in the literature.

Here, it was indeed argued that AZO-based DSSCs can progressively become competitive by taking care about the structural properties and the interfaces of the involved components in the photoanode architecture.

2. EXPERIMENTAL SECTION

ZnO:Al (AZO) layers were deposited on corning glass substrates (1737) by DC-pulsed sputter deposition using a Symmorphix 1600 equipment from a composite ZnO:Al rectangular target (98% wt ZnO and 2% wt (Al_2O_3), 64 × 55 cm^2) with an Ar flow rate of ∼20 sccm and a sputtering power of ∼350 W, at an effective temperature of 180°C (as measured by a thermostrips placed on top of the sample). By using these process parameters, a deposition rate of 0.15 nm/sec was achieved and used to deposit ∼900 nm-thick AZO layers. The electrical conductivity was evaluated by Sheet Resistance analyses which give an average value as low as 9.7 Ohm/square which corresponds to a resistivity of ∼1 mΩ × cm.

TiO_2 were deposited on AZO by using a DC reactive sputtering equipment (Kenotec) starting from a pure Titanium target. The process was carried out by applying a constant power of ∼600 W (1.24 A, 498 V, power loading 4.9 W/cm^2) for 480 s, and by setting the external heater in such a way that the value measured on the sample surface was ∼150 °C. The temperature on the sample surface was measured by using commercially available thermostrips taped on the AZO surface. An O_2/Ar flow rate ratio as low as of 5/45 sccm was set to maintain a low growth rate (3.7 nm/min) and to guarantee the proper layer stoichiometry. The process was set in the oxidised mode (in the low deposition rate regime) at a pressure of 0.85 Pa with an anode−cathode distance of 10 cm, that implies (by also considering the power loading, the deposition time and the sputtering current values used) a moderate temperature rise becaues of the plasma contribution itself if compared to the increase due to the external heating. Each deposition process is preceded by a pre-sputtering step to clean up the surface of the Ti target and to remove residual thin oxide layers. This sputtered TiO_2 layer will be called blocking layer. The TiO_2 blocking/AZO bi-layer was annealed ex-situ in dry air (N2/O2 = 78%:22%), at 200 °C for 30 min, using a Jipelec Jetfirst 150

dx.doi.org/10.1021/am4058524 | ACS Appl. Mater. Interfaces 2014, 6, 6425−6433

system equipped with a tubular infrared heating lamps and a thermocouple for an accurate control in the low temperature regime.

Alkyl-carboxylate-capped anatase TiO_2 linear nanorods (NRs) with aspect ratio 8, henceforth referred to as sample "'AR8-NRs'", were synthesized by low-temperature trimethylamine N-oxide-catalyzed hydrolysis of titanium isopropoxide (TTIP) in oleic acid;[16] in a typical synthesis, 15 mmol of TTIP were dissolved in 70 g of degassed oleic acid and the resulting solution was then reacted with 5 mL of an aqueous 2 M trimethylamine N-oxide solution at 100 °C for 96 h.

Alkyl-carboxylate-capped anatase branched TiO_2 nanostructures, namely braid-like nanorod bundles, labelled as "'BB-NRs'", were synthesized by aminolytic decomposition of titanium oleate complexes at high temperatures.[21] As a general procedure, 3 g of 1-octadecene, 3 mmol of oleyl amine, and 11 mmol of oleic acid were loaded in a three-neck flask and degassed at 120 °C for 45 min, after which the mixture is cooled down to 50 °C under N_2 flow. At this point, 1 mmol of titanium tetrachloride ($TiCl_4$) dissolved in 1 mL of 1-octadecene was added, and the flask was heated up to 290 °C at a ramp rate of 25 °C/min. After it was heated for 1 h at 290 °C, the reaction was continued by performing alternated additions of a 0.5 M oleic acid/1-octadecene solution (injected in single portion) and of a 0.5 M $TiCl_4$/1-octadecene solution (delivered at a constant rate of 0.1 mL/min by means of a syringe pump). The BB-NRs were obtained upon adding an extra 16 mmol of $TiCl_4$ after the primary injection.

After the synthesis, the TiO_2 nanocrystals were precipitated upon addition of ethanol or 2-propanol:acetone mixtures, separated by centrifugation (3000 rpm, 10′). The resulting products were easily redispersed in an apolar organic solvent, such as toluene or chloroform. Two more precipitations were performed to remove the excess surfactant residuals, preserving the sample solubility. Nanocrystal suspensions of AR8-NRs and BB-NRs (containing 4% wt/wt of TiO_2 as revealed by Inductively coupled plasma atomic emission spectroscopy) 1:1 vol/vol were stirred at 60°C for 6 h with ethylcellulose previously dissolved in toluene (10% wt/wt). Then, the solvent exchange was carried out by adding terpineol and stirring the resulting mixture for 1 h; toluene was finally removed by a rotary evaporator to obtain pastes suitable for doctor-blade deposition. The colloidal paste has the following weight percentage composition: TiO_2, 7%; organic capping residuals, 4%; ethylcellulose, 2%; terpineol, 87%.

To realise the devices, the TiO_2 blocking layer was selectively sputtered on AZO over an active area of 0.5 cm × 0.5 cm and subsequently coated with a mesoporous film of TiO_2 nanorods. The TiO_2 paste was deposited onto TiO_2 blocking/AZO/glass by doctor blading and annealed at 150 °C for 2 h followed by an UV treatment overnight (SPECTROLINE ENF-280C Ultraviolet Lamp, 8 W, with excitation wavelength centered at 365) positioned at a distance of 3 cm from the sample. This procedure was repeated several times to obtain the desired film thickness.

The TiO_2 electrodes were immersed into a solution 0.2 mM of N719 (provided by Solaronix S.A.) in a mixture of acetonitrile and *tert*-butyl alcohol (v/v, 1:1), and kept at room temperature for 14 h. The solar cells were assembled by placing a platinum-coated conducting glass (counter electrode) on photoelectrode and sealed with a 50 μm thick Surlyn hot-melt gasket. The redox electrolyte (0.1 M LiI, 0.05 M I_2, 0.6 M 1,2-dimethyl-3-propylimidazolium iodide, and 0.5 M *tert*-butylpyridine in dried acetonitrile) was introduced into the interelectrode void space through a hole predrilled on the back of the counter electrode.

The structural properties of the photoanode components (TiO_2 nanorods/TiO_2blocking/AZO/glass) were investigated by combining different analytical techniques. The microstructure of the deposited multi-layers materials was investigated by X-ray diffraction (XRD, D8-Discover Bruker AXS) and by transmission electron microscopy (TEM-JEOL JEM 2010). X-ray photoelectron spectroscopy (XPS) analyses were performed with a PHI ESCA/SAM 5600 multy technique spectrometer equipped with a monochromatized Al Ka X-ray source. UV−vis measurements were carried out on a UV−vis V-650 Jasco spectrophotometer, and the spectra were recorded with a ±0.2 nm resolution. Film surface morphology was examined by scanning electron microscopy (SEM) performed with a RAITH 150 EBL instrument. The thickness and the active area dimensions of the films were measured with a Veeco Dektak 150 profilometer.

Photocurrent−voltage IV measurements were performed using a Keithley unit (Model 2400 Source Meter). A Newport AM 1.5 Solar Simulator (Model 91160A equipped with a 300 W Xenon Arc Lamp) serving as a light source. The light intensity (or radiant power) was calibrated to 100 mW cm^{-2} using as reference a Si solar cell. The incident photon-to-current conversion efficiency (IPCE) was measured by the DC method using a computer-controlled xenon arc lamp (Newport, 140 W, 67005) coupled with a monochromator (Newport Cornerstore 260 Oriel 74125). The light intensity was measured by a calibrated silicon UV-photodetector (Oriel 71675), and the short circuit currents of the DSSCs were measured by using a dual channel optical power/energy meter (Newport 2936-C).

Electrochemical impedance spectroscopy (EIS) spectra were recorded using an AUTOLAB PGSTAT302N potentiostat operating in a two-electrode mode. Measurements were carried out under illumination at various forward bias voltages in the 300 kHz to 10 mHz frequency range and applying an AC voltage of 10 mV. Bias potentials ranged between 0.5 and 0.80 V depending on the open-circuit photopotential of the cell under illumination at 1 sun. The frequency-dependent impedance was fitted by using the Z-view software.

3. RESULTS AND DISCUSSION

3.1. TEM Analyses. The TEM cross section of the TiO_x-blocking/AZO bilayer is shown in Figure 1a. The AZO layer has a columnar structure with grains having diameters in the range of 50−150 nm. The Ti oxide layer uniformly covers the AZO substrate and has a thickness of ∼40 nm. Although the AZO surface is pretty rough (±20 nm), the coverage is conformal. A low degree of nanoporosity was introduced in the TiO_x layer to try to improve the structural coupling and the adhesion between the substrate and the mesoporous film of nanorods wich is used to complete the photoanode architecture. Nevertheless, in the deposition procedure some

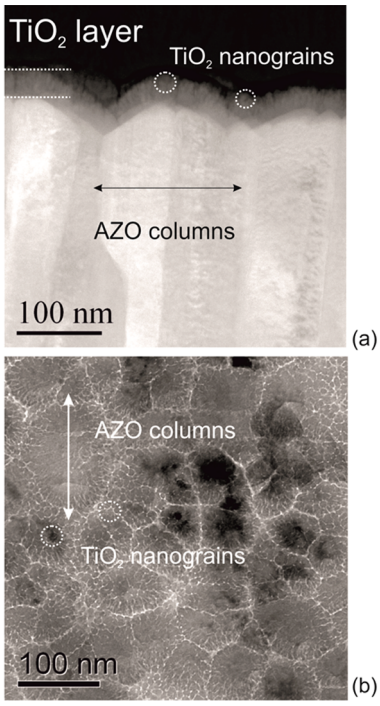

Figure 1. (a) Cross-section and (b) plan-view TEM analyses of the TiO_2-blocking/AZO bilayer (as deposited). The TiO_2-blocking layer creates a conformal coverage over the faceted AZO surface.

dx.doi.org/10.1021/am4058524 | ACS Appl. Mater. Interfaces 2014, 6, 6425−6433

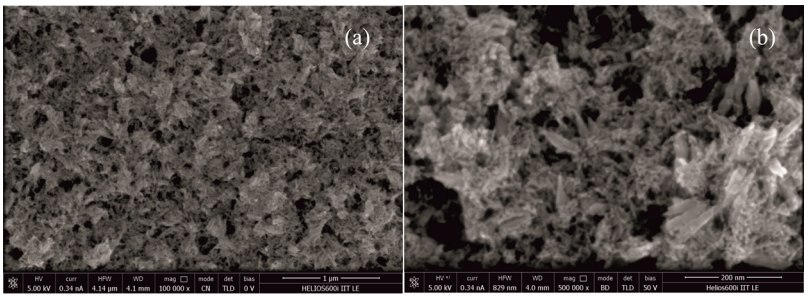

Figure 2. SEM images of the TiO_2 nanorods deposited over the TiO_2-blocking/AZO bilayer: (a) Mag = 100000× and (b) Mag = 500000 × 3.3.

precautions were taken in order to protect the AZO surface against corrosion consisting of a flash of pure titanium which was deposited at the very beginning of the process. Detailed studies on the properties of the TiO_2 blocking layer and on their tuning through deposition parameters are reported elsewhere[4,5]

The Ti oxide grains, after deposition, are 8−15 nm large and are uniformly distributed over the surface of the AZO columns, as shown in Figure 1b. The composition of the Ti oxide layer will be discussed in what follows.

3.2. SEM Analyses. Over the TiO_2-blocking/AZO bilayer, a mesoporous film of TiO_2 nanorods (4 μm thick) was deposited by a doctor blade technique. The nanorod-based films are characterized by a good homogeneity and the absence of aggregates, as shown by the SEM analyses in Figure 2a. The hydrophobic oleate surfactant shell employed in the synthesis plays a pivotal role in maintaining good nanoparticle dispersion during the post-synthesis process steps, so the elongated nanocrystal morphology and the original size appeared to have been adequately preserved. SEM images (Figure 2b) revealed the presence of a "bone structure" of about 150-nm-sized nanorods which provide huge surface area to the working electrode.

3.3. XPS Analyses. The TiO_2 nanorods have been analyzed by X-ray photoelectron spectroscopy (XPS) before and after the low temperature "sintering" process and the UV treatment. The XPS-spectra of both samples show the presence of carbon, oxygen, and titanium with the relative atomic percentages reported in Table 1:

Table 1. Atomic Percentages As Revealed by XPS Measurements before and after the Low Temperature/UV "Sintering" Process

	before sintering (%)	after sintering (%)
C 1s tot	64.6	20.8
O 1s tot	33.2	56.2
Ti 2p	2.2	23.0

The data demonstrate a noticeable difference in the surface composition of the TiO_2 nanorods before and after the treatment. In particular, a strong reduction of the total adventitious carbon amount is observed after the "sintering" process, thus suggesting a significant removal of the organic components with the thermal/UV treatment. As a consequence of this, the relative atomic percentage of titanium increases noticeably after the process.

Figure 3 shows the C 1s, O 1s, and Ti 2p XPS regions related to the TiO_2 nanorods before (a, b, c) and after (d, e, f) the low temperature "sintering". Before the treatment, the C 1s region (Figure 3a) shows, in addition to the ubiquitous component at 285.0 eV resulting from organic and adventitious C−C, C−H carbons, a large contribution centered at 287.0 eV due to the carbons bonded to oxygen from the organic matrix of the source TiO_2 paste. After the thermal treatment at 150 °C and UV irradiation, the C 1s region (Figure 3d) is strongly modified. The band centered at 287.0 eV is no longer present, thus indicating the removal of the organic components. The region after sintering appears very similar to that obtained from TiO_2 layers grown by sputtering (e.g., the buffer layer, not shown) since it presents a main signal positioned at 285.0 eV and a well-resolved band lying at 288.8 eV. We attribute the observed C 1s contributions to the adventitious carbon (centered at 285.0 eV) and carbonates (288.8 eV).

In accordance with what observed in the C 1s region, the O 1s spectrum of the untreated TiO_2 nanorods (Figure 3b) is strongly affected by the presence of the organic components, as demonstrated by the large band centered at 533.4 eV because of the C−OH and C−O−C bonds. In addition, as visible in the figure, a low intense band lying at 530.0 eV, relative to the oxygen of the TiO_2 structure, is observed. After the combined thermal and UV treatments (Figure 3f), the large band at 533.4 eV is not long visible and the contribution related to the titanium oxide results predominant. The shoulder at higher binding energy (531.6 eV) is referred to the presence of carbonates species, consistently with what observed in the C 1s region together with surface Ti−OH terminations.

In the XP spectra of both the samples, the titanium region shows the typical spin-orbit doublet resulting from the Ti $2p_{3/2}$ and Ti $2p_{1/2}$ contributions. The Ti $2p_{3/2}$ component lies at 458.6 eV, a value consistent with the presence of the metal in the +4 oxidation state. The ratio between the integrated intensities of the titanium signal and the oxygen component at 530.0 eV results very close to the value expected from the TiO_2 stoichiometric formula, being ∼2.0 for both the untreated and treated TiO_2 nanorods.

3.4. UV−vis Transmittance Analyses. The AZO transmittance on glass, before Ti-oxide deposition, was evaluated in the range between 300 and 800 nm (Figure 4). The maximum value is around 80%. Adding the 40 nm-thick Ti oxide layer, conformal over the AZO surface, causes a certain reduction of the transmittance, with maximum values around the 70% at wavelengths longer than 450 nm, which correspond to the region of maximum absorption of the N719 dye.

The layer transmittance can be further improved by annealing the Ti-oxide/AZO bilayer at 200°C. This phenomenon was explained by a thermally induced process of defects recovery in the semiconductor layers.[22,23] As a consequence of that, the $T(\lambda)$ curve becomes steeper above the absorption threshold (critical region indicated in the figure) and shifts

dx.doi.org/10.1021/am4058524 | ACS Appl. Mater. Interfaces 2014, 6, 6425−6433

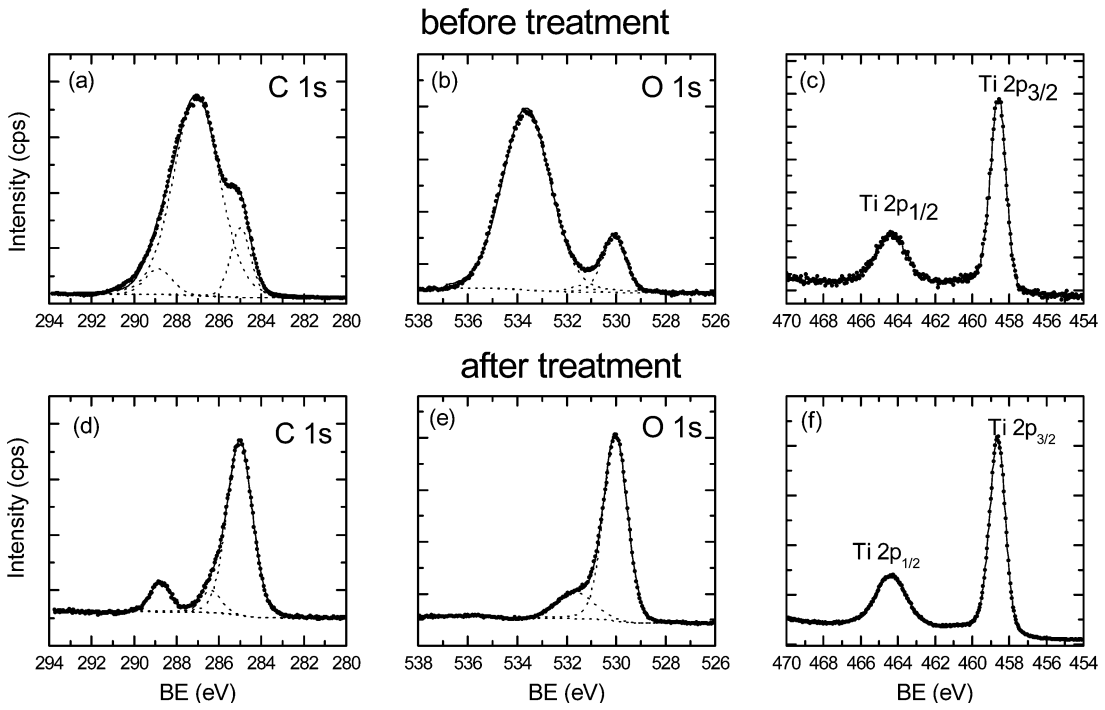

Figure 3. X-ray photoelectron spectroscopy in the C 1s, O 1s, and Ti 2p regions of the TiO_2 nanorods before (a, b, c) and after (d, e, f) the sintering treatment.

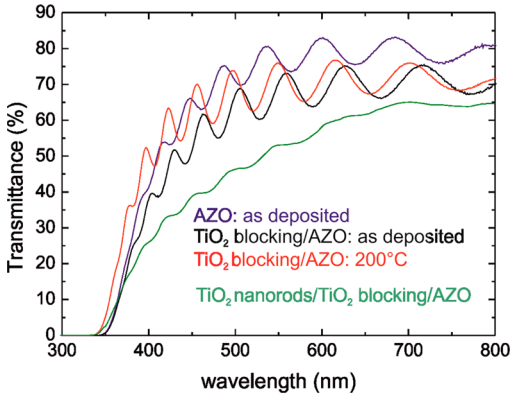

Figure 4. Optical transmittance of TiO_2-blocking/AZO bilayer left as deposited or treated at 200 °C, compared to that of the AZO layer alone. The transmittance of the complete stack, with the nanorods deposited over the TiO_2-blocking/AZO bilayer, is also shown.

towards lower wavelength. The evidence of the occurrence of a process of structural defects recovery, which thus causes a narrowing of the density of optically efficacious states near the gap, is in agreement with the occurrence of a severe structural modification induced by the thermal treatments as will be described by the X-ray diffraction results. The optical transmittance was further reduced after nanorods deposition.

3.5. X-ray Diffraction Analyses. The crystallographic orientation of the AZO columns, shown in Figure 1a, was investigated by $2\theta-\omega$ and rocking curve XRD analyses. The $2\theta-\omega$ scan has an intense peak associated with the (0002) planes of the zincite hexagonal structure, with a related rocking curve (Figure 5a) having a full width at half maximum (FWHM) of 8.4°, offaxis≅0°. The AZO layer is thus textured, with the [0002] as the preferential growth axis.

The Ti-oxide layer deposited by sputtering on AZO is not amorphous (fig.5b). Rather it has small crystallized grains of TiO_2 in the anatase and rutile polymorphisms already after deposition, although the deposition temperature is under the threshold for crystallization (T<200°C see Introduction). The peaks are pretty wide due to the fact that the size of the domains is small (10 ± 2 nm, following the Debye-Scherrer formula).

After annealing the TiO_2-blocking/AZO bilayer at a temperature slightly above that of deposition (200 °C vs 150 °C) but for a prolonged time, the composition of the blocking layer settles in the anatase polymorphism. The diffraction peaks are indexed in Figure 5b, and the fitting parameters are reported in Table 2.

From Table 2, related to the 200 °C annealed TiO_2-blocking/AZO bilayer, the following can be noted: (1) Anatase polymorphism prevails at this temperature. The starting very little amount of rutile was lost during annealing, as expected on the basis of its instability at larger size at low temperatures.[24] (2) The anatase grains have grown during annealing. (3) The texture coefficient is, for some planes, higher than that expected in that range (0.2) (texture coefficient $J = (I_{hkl}/I^*_{hkl}/\Sigma_{hkl}(I_{hkl}/I^*_{hkl}))$, where I^* is the expected intensity in a reference powder). Anatase nucleation and growth triggered by preferentially oriented AZO substrates (e.g., [0001]) is a result expected on the basis of our previous data, at least for annealing up to 200 °C.[4,25] Some differences in the texturing properties of this TiO_2 layer can be encountered by slightly changing the surface exposed by the AZO to the TiO_2 deposition process, such as it can result from a different off axis in the AZO growth direction (under investigation).

The same structural analysis was done after nanorods deposition, on both the TiO_2-blocking/AZO bilayer substrates (as deposited and annealed at 200 °C, before nanorods deposition). The results are shown in Figure 5c and are independent of the substrate used. The anatase is the unique polymorphism present in the mesoporous array of nanorods.

dx.doi.org/10.1021/am4058524 | ACS Appl. Mater. Interfaces 2014, 6, 6425−6433

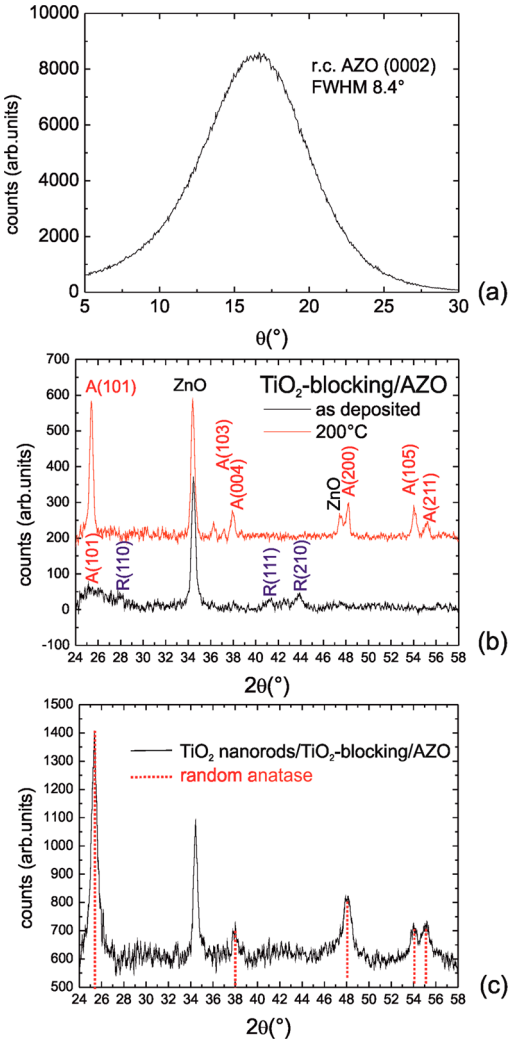

Figure 5. XRD analyses of (a) the AZO substrate (rocking curve), (b) the TiO_2-blocking/AZO bilayer (grazing incidence 0.4°), and (c) the TiO_2 nanorods/TiO_2-blocking/AZO multilayer (grazing incidence 0.4°), with the blocking/AZO bilayer left as deposited or treated at 200°C. The AZO peaks in panel c are because the active area covered by the nanorods was smaller than the beam size. The annealing process at low T changes the blocking layer structure and stabilizes the anatase polymorphism. The nanorods are in the anatase form and are randomly oriented.

Table 2. XRD Peak Parameters of the TiO_2-Blocking Layers All Related to the Anatase Polymorphism after Ex Situ Annealing at 200 °C (30′)

2θ	hkl	d (Å)	grain diameter (nm)	texture coefficient
25.36	101	3.51	21	0.35
37.93	004	2.37	13	0.18
48.26	200	1.88	32	0.10
54.05	105	1.70	46	0.24
55.06	211	1.67	31	0.14

All the expected diffraction peaks are present and the relative ratios of the registered intensities closely approach those of a randomly oriented anatase grain system. The average size of the domains, as extracted by the FWHM of the peaks, is 17 ± 5 nm. This value accounts for the two components of the nanorods array diameter (see section 3.2).

3.6. DSSC Electrical Characterization. To evaluate the eventual benefits in using the structurally optimized TiO_2-blocking/AZO bilayer as substrate for the TiO_2 nanorods, $J-V$ analyses were done on the cells having the bilayer left as deposited or treated at 200 °C before nanorods deposition and dye loading. The results are shown in Figure 6a.

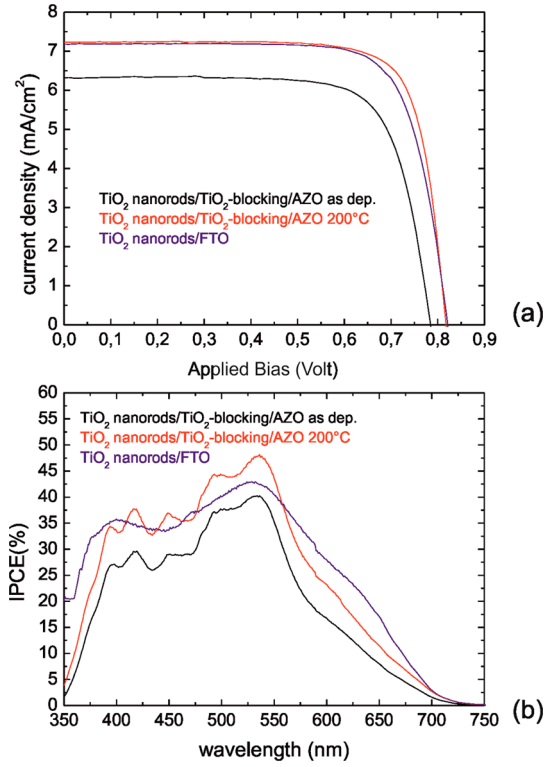

Figure 6. (a) $J-V$ and (b) IPCE analyses related to the TiO_2 nanorods/TiO_2-blocking/AZO bilayer-based DSSC having the TiO_2-blocking/AZO bilayer left as deposited or treated at 200 °C. For comparison, a reference cell with the TiO_2 nanorods deposited on FTO is also reported. The nanorods layer thickness is ~4μm. The maximum registered efficiency was 4.57%. The current maximum efficiency value reported in the literature for AZO-based DSSC is 3.8 % (for 10 μm nanopastes, sintered at 450 °C, and sensitized by N719).

Here, we would like to point out that our attempt to realise a reference cell, without the TiO_2-blocking layer, over the AZO substrate gave modest results (η = 0.44%, V_{oc} = 0.604, J_{sc} = 1.23, FF = 0.60) mainly because of the poor adhesion of nanorods-based film to AZO substrate. Therefore, an intermediate TiO_2 layer is strictly mandatory in this approach, also necessary to protect the AZO layer against the electrolytic solution. In this respect instead, the two cells, having the TiO_2-blocking/AZO bilayer left as deposited or treated at 200 °C, exhibited a good adhesion between the components. Moreover, both of them showed competitive electrical performances. The results are shown in Table 3: because of the implementation of the annealed TiO_2-blocking layer, the J_{SC} was increased from 6.31 to 7.23 mA/cm^2, and this was attributed to a superior ability to collect photoinjected electrons as an effect of the reduction of back reactions events. An increase in V_{OC} (from 0.784 to 0.810 V) was observed for the thermally treated substrate, also due to the reduction of the recombination processes with the electrolyte (see EIS analyses). A maximum efficiency as high as the 4.6% was registered by employing the bilayer pre-treated at 200°C and by using a 4 μm-thick

dx.doi.org/10.1021/am4058524 | ACS Appl. Mater. Interfaces 2014, 6, 6425−6433

Table 3. Cell Parameters As a Function of the TiO_2-Blocking/AZO Preparation Procedure[a]

	substrate	substrate annealing (°C)	mesoporous film	mesoporous film annealing (°C)	η (%)	V_{oc} (V)	J_{sc} (mA/cm^2)	FF
as deposited substrate	TiO_2 blocking/AZO		TiO_2 nanorods (4 μm)	150	**3.71**	0.784	6.31	0.75
thermally treated substrate	TiO_2 blocking/AZO	200	TiO_2 nanorods (4 μm)	150	**4.57**	0.810	7.23	0.78
our reference on AZO	AZO		TiO_2 nanorods (4 μm)	150	**0.44**	0.604	1.23	0.60
our reference on FTO	FTO	450	TiO_2 nanorods (4 μm)	150	**4.45**	0.806	7.18	0.77
ref 10	Nb-TiO_2 blocking/AZO	450	TiO_2 nanoparticles (10 μm)	450	**3.78**	0.740	8.52	0.60
ref 11	Nb-TiO_2 blocking/AZO/Ag/AZO		TiO_2 nanoparticles (16 μm)	450	**3.25**	0.795	5.84	0.70

[a]The nanorod layer is 4 μm-thick. The fourth line refers to the cell using FTO as substrate. In the table, our data were also compared with the current maximum efficiency values for AZO-based DSSCs reported in the literature.

mesoporous nanorods-based photoanodes. In the literature, a maximum efficiency of 3.8% is currently reported for AZO-based DSSC by using a standard 10 μm thick TiO_2 photoelectrode sintered at 450 °C.[10]

In Table 3, for comparison, the photovoltaic parameters for a reference cell with the TiO_2 nanorods deposited on commercially available FTO (R_s = 15 ohm/sq, deposition temperature >450 °C) are also reported. Such device showed similar power conversion efficiency, thus demonstrating the effectiveness of our strategy. The superior J_{SC} value for the bilayer pre-treated at 200 °C also emerged from the incident photon-to-current conversion efficiency (IPCE) spectra (Figure 6b), which showed ∼47% efficiency at 550 nm for the 200 °C device compared to the ∼40% obtained for the device based on not annealed blocking layer.

To investigate the electrochemical characteristics of the two different electrodes, electrochemical impedance spectroscopy (EIS) were carried out, and the results are shown in Figure 7. The arcs observable in the Nyquist diagram (Figure 7a) reveal the existence of defined electrochemical interfaces with different time constants.[26] The depressed semicircle in the high frequency region (the left one) arises from parallel connection between the capacities of the counter electrode and the TCO/electrolyte interface at the bottom of the TiO_2 film and the resistance given by the sum of the counter electrode/electrolyte and the TCO/TiO_2 interface (R_{CE}). The largest medium frequency arc is associated with the parallel combination of recombination resistance (R_{CT}) at TiO_2/electrolyte interface and recombination resistance (R_{TCO}) at the TCO/electrolyte interface combined with the chemical capacitance (C_μ) of electrons in TiO_2. A minor lowest-frequency arc (in the rightmost region of the diagram, not totally detected here) is attributed to the impedance of diffusion of redox species in the electrolyte (R_D). Finally the displacement of the arc is attributed to the contribution of the total series resistance (R_{series}) of the wiring, AZO, buffer layer resistances within the TiO_2 film.[27]

Since all the devices were fabricated and tested in the same conditions, here, we argue that the differences in the TiO_2 blocking layers play the major role on the electrochemical parameters. We indeed noted that the high frequency intercepts of 200 °C-AZO/TiO_2-blocking DSCC shifted backwards, attesting a reduction of the buffer layer resistance, in accordance with the observed reduction of the AZO (alone) sheet resistance, which decreased from ∼10 to ∼7 ohm/sq upon 200 °C annealing; this issue positively impacted on the registered higher fill factor of the device (see Table 3).[28]

Moreover, from the analysis of the Nyquist plots of EIS spectra in the full range of potentials applied, we were not able to distinguish the transport resistance. This means that the transport resistance is much smaller than recombination resistance, and thus the presence of the blocking layer does not negatively affect the electron diffusion length, which is instead large enough to guarantee an effective charge collection.[29] To a deeper understanding of the processes involved in the charge collection, some significant electrochemical parameters were plotted in Figure 7b and 7c as a function of the corrected potential to account for the losses because of the series resistance R_s (which provides a potential drop not associated with the displacement of the Fermi level). The corrected potential, V_{corr} was calculated from the applied potential, V_{appl}, as following:

$$V_{corr} = V_{appl} - J \times A \times R_s$$

where A is projected area of cell and J is the flowing current density.[30]

In Figure 7b, the measured capacitance C_{meas} versus the corrected potential is shown. It presents two-regimes behaviour: at lower potentials the capacitance is dominated by the Helmholtz layer at the AZO-buffer layer/electrolyte interface while at intermediate and high potentials C_{meas} exhibits a characteristic exponential rise of C_μ, indicating the occurrence of a charging phenomenon in the semiconductor nanocrystalline matrix. Since the chemical capacitance of the two different samples is comparable, we conclude that the conduction band in the semiconductor nanoparticles does not present a relevant shift.[20] This allows a better comparison of the recombination resistance of the two samples.

In Figure 7c, the charge transfer resistance, R_{ct} is plotted as a function of the corrected voltage. The highest R_{ct} values were registered for the cell having the AZO/TiO_2-blocking pre-treated at 200 °C, and this attests that injected electrons scarcely undergo recombination with the oxidized species of the redox solution present in the electrolyte.[31] This implies that, in especially in this case, the parasitic diode works less efficiently thanks to the efficacious contribution of the pretreated TiO_2-blocking layer.[32] The enhanced electron recombination resistance reflects on the highest value of V_{OC} registered in that cell and may be explained by considering the better degree of crystallinity of the pre-treated blocking layer, which would

dx.doi.org/10.1021/am4058524 | ACS Appl. Mater. Interfaces 2014, 6, 6425−6433

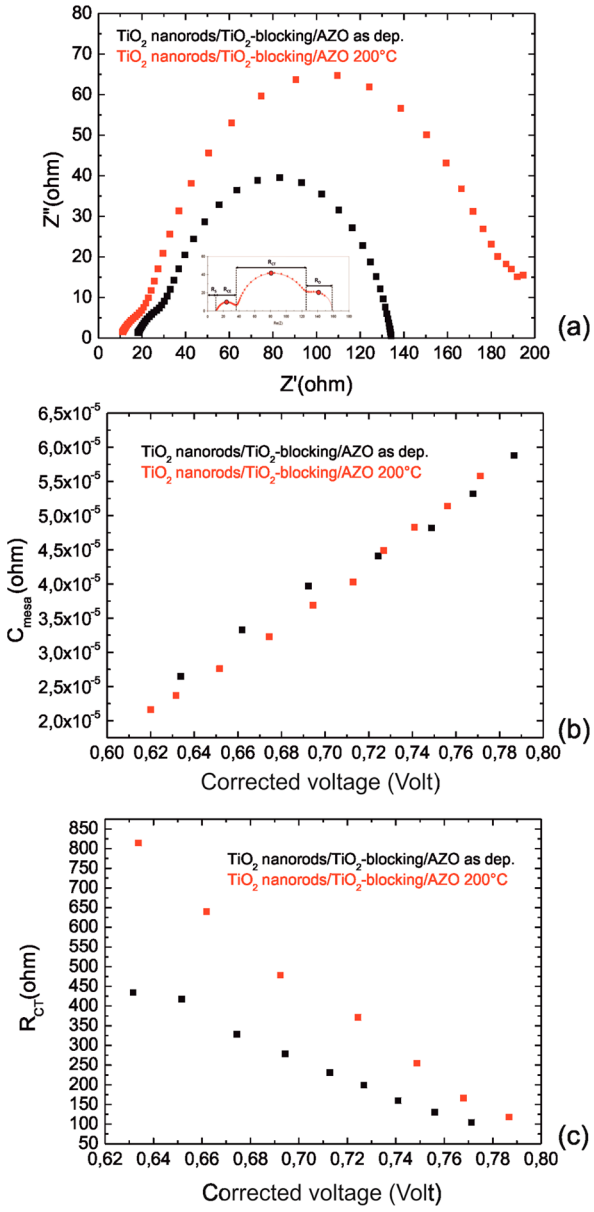

Figure 7. (a) Impedance spectra of DSCs at a potential close to V_{oc} (−0.75 V) measured under 1 sun illumination for the samples with the AZO/TiO_2-blocking bilayer left as deposited or annealed at 200 °C. (b) Electrode capacitance and (c) recombination resistance obtained by electrochemical impedance spectroscopy under 1 sun illumination; the capacitance and recombination resistance are plotted versus the potential drop at the sensitized electrode.

reasonably assure a fast transfer of the photoinjected electrons to the AZO substrate.

CONCLUSIONS

In this paper, we proposed a competitive low-temperature approach to realise innovative photoanodes consisting of a highly transparent AZO film, a TiO_2 blocking layer and a mesoporous TiO_2 nanorods-based film processed at $T \leq 200$ °C. It was shown that the use of this multilayered nanostructure can assure competitive performances to the solar cell. With respect to the literature, the TiO_2-blocking layer we used is thinner, undoped, and structurally optimized at $T \leq 200$ °C. The layer, after a postdeposition soft annealing at 200 °C, is in the anatase polymorphism, despite the low temperature process, and has a nanocrystalline habit. It was demonstrated that such a layer serves several purposes: to guarantee the adhesion between the nanorods and the AZO substrate; to reduce the parasitic diode current (high recombination resistance); and to protect the AZO surface against corrosion. It was also demonstrated that the use of a 4 μm-thick mesoporous TiO_2 nanorods-based photoanode realised at $T <$ 200 °C, combined with the use of the TiO_2-blocking/AZO bilayer pre-treated at T = 200 °C, allows exceeding the current limit for the cell efficiency (3.8%), which was instead got by applying a thermal budget of 450 °C over a 10μm-thick TiO_2 mesoporous film deposited over a 100-nm-thick Nb-doped TiO_2 layer. Our value was as high as the 4.6% ($T \leq 200$ °C; 4-μm-thick nanorods; undoped 40-nm-thick TiO_2layer sputtered on AZO). This result can be likely related to some peculiar characteristics of this new multilayer structure: (i) the uniformity, conformity, and degree of crystallinity of the blocking layer; (ii) the good conductivity of the TiO_2-blocking/AZO bilayer interface; (iii) the good light-harvesting and electron transport capabilities of the nanorod-based mesoporous layer which, upon a mild annealing treatment (<200 °C) and a simple UV irradiation, resulted in a product free from organics and suitable for efficient dye solar cells.

An accurate control of the deposition parameters and of the structural properties of the photoanode components thus prospects a further improvement of the AZO-based cells performances also on newly designed high quality plastics substrates.

AUTHOR INFORMATION

Corresponding Author

*E-mail: alessandra.alberti@imm.cnr.it.

Author Contributions

A.A. and L.D.M. contributed equally.

Notes

The authors declare no competing financial interest.

ACKNOWLEDGMENTS

The authors would like to thank C. Bongiorno (CNR-IMM) for TEM analyses, B. Cafra (STMicroelectronics) for support in AZO depositions, and M. Italia (CNR-IMM) for the RTA processes. This work was partially supported by the CNR Italian project EFOR-CABIR (Energia da Fonti Rinnovabili-FotovoltaiCo OrgAnico/IBrido dI Terza GeneRazione) CUP B51J10001290001 and by MIUR-PRIN 2010-2011 Project No. 20104XET32 "DSSCX". Daunia Wind is gratefully acknowledged for funding.

REFERENCES

(1) Gratzel, M. Solar Energy Conversion by Dye-Sensitized Photovoltaic Cells. *Inorg.Chem.* **2005**, *44*, 6841−6851.

(2) Pellegrino, G.; Alberti, A.; Condorelli, G.G.; Giannazzo, F.; La Magna, A.; Paoletti, A.M.; Pennesi, G.; Rossi, G.; Zanotti, G. Study of the Anchoring Process of Tethered Unsymmetrical Zn-Phthalocyanines on TiO_2 Nanostructured Thin Films. *J. Phys. Chem. C* **2013**, *117*, 11176−11185.

(3) Liu, H.; Avrutin, V.; Izyumskaya, N.; Ozgur, U.; Morkoc, H. Transparent Conducting Oxides for Electrode Applications in Light Emitting and Absorbing Devices. *Superlattices Microstruct.* **2010**, *48*, 458−484.

(4) Alberti, A.; Bongiorno, C.; Pellegrino, G. Anatse/Rutile Nucleation and Growth on (0002) and (11$\bar{2}$0) Oriented ZnO:Al/

Glass Substrates at 150 °C. *Thin Solid Films* **2013**, DOI: 10.1016/j.tsf.2013.10.006.
(5) Pellegrino, G.; Condorelli, G.G.; De Rossi, F.; Brown, T.; Giovenale, F.; Bongiorno, C.; Alberti, A. Thermally Induced Structural Modifications of Nano-Sized Anatase Films and the Effects on the Dye−TiO_2 Surface Interactions. *Appl. Surf. Sci.* **2014**, *296*, 69−78.
(6) Yu, H.; Zhang, S.; Zhao, H.; Xue, B.; Liu, P.; Will, G. High Performance TiO_2 Photoanode with an Efficient Electron Transport Network for Dye-Sensitized Solar Cells. *J. Phys. Chem. C* **2009**, *113*, 16277−16282.
(7) Wua, M.-S.; Tsaia, C.-H.; Jowa, J.-J.; Weib, T.-C. Enhanced Performance of Dye-Sensitized Solar Cell via Surface Modification of Mesoporous TiO_2 Photoanode with Electrodeposited Thin TiO_2 Layer. *Electrochim. Acta* **2011**, *56*, 8906−8911.
(8) Wu, M.-S.; Tsai, C.-H.; Wei, T.-C. Electrochemical Formation of Transparent Nanostructured TiO_2 Film as an Effective Bifunctional Layer for Dye-Sensitized Solar Cells. *Chem. Commun.* **2011**, *47*, 2871−2873.
(9) Miyoshi, K.; Numao, M.; Ikegami, M.; Miyasaka, T. Effect of Thin TiO_2 Buffer Layer on the Performance of Plastic-Based Dye-Sensitized Solar Cells Using Indoline Dye. *Electrochemistry* **2008**, *76*, 158−160.
(10) Alberti, A.; Pellegrino, G.; Condorelli, G.G.; Bongiorno, C.; Morita, S.; La Magna, A.; Miyasaka, T. Efficiency Enhancement in ZnO:Al-Based Dye-Sensitized Solar Cells Structured with Sputtered TiO_2 Blocking Layers. *J. Phys. Chem. C* **2014**, DOI: 10.1021/jp411811q.
(11) Noh, J. H.; Han, S.; Lee, S.; Kim, D. H.; Park, J. H.; Park, S.; Kim, J. Y.; Jung, H. S.; Hong, K. S. A Newly Designed Nb-Doped TiO_2/Al-Doped ZnO Transparent Conducting Oxide Multilayer for Electrochemical Photoenergy Conversion Devices. *J. Phys. Chem. C* **2010**, *114*, 13867−13871.
(12) Qi, J.-H.; Li, Y.; Duong, T.-T.; Choi, H.-J.; Yoon, S.-G. Dye-Sensitized Solar Cell Based on AZO/Ag/AZO Multilayer Transparent Conductive Oxide film. *J. Alloys Compd.* **2013**, *556*, 121−126.
(13) Gago, R.; Redondo-Cubero, A.; Vinnichenko, M.; Vazquez, L. Annealing of Heterogeneous Phase TiO_2 Films: An X-Ray Absorption and Morphological Study. *Chem. Phys. Lett.* **2011**, *511*, 367−371.
(14) Gago, R.; Vinnichenko, M.; Redondo-Cubero, A.; Czgany, Z.; Vazquez, L. Surface Morphology of Heterogeneous Nanocrystalline Rutile/Amorphous Anatase TiO_2 Films Grown by Reactive Pulsed Magnetron Sputtering. *Plasma Processes Polym.* **2010**, *7*, 813−823.
(15) Musil, J.; Herman, D.; Sicha, J. Low-Temperature Sputtering of Crystalline TiO_2 films. *J. Vac. Sci. Technol., A* **2006**, *24*, 521−528.
(16) De Marco, L.; Manca, M.; Buonsanti, R.; Giannuzzi, R.; Malara, F.; Pareo, P.; Martiradonna, L.; Giancaspro, N.M.; Cozzoli, P.D.; Gigli. High-Quality Photoelectrodes Based on Shape-Tailored TiO_2 Nanocrystals for Dye-Sensitized Solar Cells, G. *J. Mater. Chem.* **2011**, *21*, 13371−13379.
(17) Agosta, R.; Giannuzzi, R.; De Marco, L.; Manca, M.; Belviso, M.; Cozzoli, P. D.; Gigli, G. Electrochemical Assessment of the Band-Edge Positioning in ShapeTailored TiO2-Nanorod-Based Photoelectrodes for Dye Solar Cells. *J. Phys. Chem. C* **2013**, *117*, 2574−2583.
(18) De Marco, L.; Manca, M.; Giannuzzi, R.; Belviso, M. R.; Cozzoli, P. D.; Gigli, G. Shape-Tailored TiO_2 Nanocrystals with Synergic Peculiarities As Building Blocks for Highly Efficient Multi-stack Dye Solar Cells. *Energy Environ. Sci.* **2013**, *6*, 1791−1795.
(19) Zardetto, V.; Brown, T. M.; Reale, A.; Di Carlo, A. Substrates for Flexible Electronics: A Practical Investigation on the Electrical, Film Flexibility, Optical, Temperature, and Solvent Resistance Properties. *J. Polym. Sci., Part B: Polym. Phys.* **2011**, *49*, 638−648.
(20) MacDonald, W. A.; Looney, M. K.; MacKerron, D.; Eveson, R.; Adam, R.; Hashimoto, K.; Rakos, K. Latest Advances in Substrates for Flexible Electronics. *J. Soc. Inf. Disp.* **2007**, *15/12*, 1075−1083.
(21) Buonsanti, R.; Carlino, E.; Giannini, C.; Altamura, D.; De Marco, L.; Giannuzzi, R.; Manca, M.; Gigli, G.; Cozzoli, P. D. Hyperbranched Anatase TiO_2 Nanocrystals: Nonaqueous Synthesis, Growth Mechanism, and Exploitation in Dye-Sensitized Solar Cells. *J. Am. Chem. Soc.* **2011**, *133*, 19216−19239.
(22) Mo, S.-D.; Ching, W. Y. Electronic and Pptical Properties of Three Phases of Titanium Dioxide: Rutile, Anatase, and Brookite. *Phys. Rev. B* **1995**, *51*, 13023−13032.
(23) Landmann, M.; Köhler, T.; Köppen, S.; Rauls, E.; Frauenheim, T.; Schmidt, W. G. Fingerprints of Order and Disorder in the Electronic and Optical Properties of Crystalline and Amorphous TiO_2. *Phys. Rev. B* **2012**, *86*, No. 064201.
(24) Hanaor, D. A. H.; Sorrell, C. C. Review of the Anatase to Rutile Phase Transformation. *J. Mater. Sci.* **2011**, *46*, 855−874.
(25) Pellegrino, G.; Bongiorno, C.; Ravesi, S.; Alberti, A. Fiber Texturing in Nano-Crystalline TiO_2 Thin Films Deposited at 150 °C by DC Reactive Sputtering on Fiber-Textured [0001] ZnO:Al Substrates. *J. Phys. D: Appl. Phys.* **2012**, *45*, No. 355301.
(26) Barsoukov, E.; Macdonald, J. R. *Impedance Spectroscopy: Theory, Experiment, and Applications*, 2nd ed; John Wiley & Sons: Hoboken, NJ, 2005.
(27) Longo, C.; Nogueira, A. F.; De Paoli, M. A.; Cachet, H. Solid-State and Flexible Dye-Sensitized TiO_2 Solar Cells: a Study by Electrochemical Impedance Spectroscopy. *J. Phys. Chem. B* **2002**, *106*, 5925−5930.
(28) Koide, N.; Islam, A.; Chiba, Y.; Han, L. Improvement of Efficiency of Dye-Sensitized Solar Cells Based on Analysis of Equivalent Circuit. *J. Photochem. Photobiol.* **2006**, *A* (182), 296−305.
(29) Bisquert, J. Theory of the Impedance of Electron Diffusion and Recombination in a Thin Layer. *J. Phys. Chem. B* **2002**, *106*, 325−333.
(30) Fabregat-Santiago, F.; Garcia-Belmonte, G.; Mora-Sero, I.; Bisquert. Characterization of Nanostructured Hybrid and Organic Solar Cells by Impedance Spectroscopy. *J. Phys. Chem. Chem. Phys.* **2011**, *13*, 9083−9118.
(31) Wu, M.-S.; Tsai, C.-H.; Wie, T.-C. Electrochemical Formation of Transparent Nanostructured TiO_2 Film as an Effective Bifunctional Layer for Dye-Sensitized Solar Cells. *Chem. Commun.* **2011**, *47*, 2871−2873.
(32) Góes, M. S.; Joanni, E.; Muniz, E.C.; Savu, R.; Habeck, T. R.; Bueno, P. R.; Fabregat-Santiago, F. Impedance Spectroscopy Analysis of the Effect of TiO_2 Blocking Layers on the Efficiency of Dye Sensitized Solar Cells. *J. Phys. Chem. C* **2012**, *116*, 12415−12421.